EARTH SURFACE PROCESSES AND LANDFORMS
Earth Surf. Process. Landforms (2020)

Published online in Wiley Online Library
(wileyonlinelibrary.com) DOI: 10.1002/esp.4830

Large wood inhibits debris flow runout in forested southeast Alaska

Adam M. Booth,[1]* Christian Sifford,[1] Bryce Vascik,[1] Cora Siebert[1] and Brian Buma[2]
[1] Department of Geology, Portland State University, Portland, OR USA
[2] Department of Integrative Biology, University of Colorado, Denver, CO USA

Received 9 August 2019; Revised 21 January 2020; Accepted 28 January 2020

*Correspondence to: Adam M. Booth, Department of Geology, Portland State University, 17 Cramer Hall, 1721 SW Broadway, Portland, OR 97201, USA. E-mail: boothad@pdx.edu

ESPL
Earth Surface Processes and Landforms

ABSTRACT: Due to their potentially long runout, debris flows are a major hazard and an important geomorphic process in mountainous environments. Understanding runout is therefore essential to minimize risk in the near-term and interpret the pace and pattern of debris flow erosion and deposition over geomorphic timescales. Many debris flows occur in forested landscapes where they mobilize large volumes of large woody debris (LWD) in addition to sediment, but few studies have quantitatively documented the effects of LWD on runout. Here, we analyze recent and historic debris flows in southeast Alaska, a mountainous, forested system with minimal human alteration. Sixteen debris flows near Sitka triggered on August 18, 2015 or more recently had volumes of 80 to 25 000 m^3 and limited mobility compared to a global compilation of similarly-sized debris flows. Their deposits inundated 31% of the planimetric area, and their runout lengths were 48% of that predicted by the global dataset. Depositional slopes were 6°–26°, and mobility index, defined as the ratio of horizontal runout to vertical elevation change, ranged from 1.2 to 3, further indicating low mobility. In the broader southeast Alaskan region consisting of Chichagof and Baranof Islands, remote sensing-based analysis of 1061 historic debris flows showed that mobility index decreased from 2.3–2.5 to 1.4–1.8 as average forest age increased from 0 to 416 years. We therefore interpret that the presence of LWD within a debris flow and standing trees, stumps, and logs in the deposition zone inhibit runout, primarily through granular phenomena such as jamming due to force chains. Calibration of debris flow runout models should therefore incorporate the ecologic as well as geologic setting, and feedbacks between debris flows and vegetation likely control the transport of sediment and organic material through steep, forested catchments over geomorphic time. © 2020 John Wiley & Sons, Ltd.

KEYWORDS: debris flow; ecogeomorphology; landslide runout; Sitka; large woody debris

Introduction

Debris flows are geologic hazards (e.g. Jakob and Hungr, 2005) and important geomorphic agents that incise and transport sediment through steep channels (Eaton *et al.*, 2003; Anderson *et al.*, 2015). They are especially hazardous to humans because of their high velocities and long runout distances, which often result in hundreds of fatalities around the world per year (Dowling and Santi, 2014). Over geologic time, channels carved by repeated debris flows can contain most of a landscape's topographic relief and are characterized by different slope-area scaling than fluvial channels or hillslopes, demonstrating the unique influence of debris flows on setting topographic form (Stock and Dietrich, 2003, 2006; Penserini *et al.*, 2017). Debris flows can also affect downstream channel morphology by altering grain size distributions, sediment loads, and in-stream wood (Benda and Dunne, 1997; Lancaster *et al.*, 2001; Montgomery *et al.*, 2003; May and Gresswell, 2002). It is therefore necessary to better understand the mechanisms that control debris flow runout to improve estimates of debris flow hazards, manage risk, and interpret landscape evolution in steep mountainous regions.

Two widely applied and practical measures of debris flow mobility that often form the basis of hazard analyses are the planimetric area inundated by the flow and the maximum horizontal distance it travels (Rickenmann, 2005). Both these measures systematically increase with volume over many orders of magnitude ranging from small alpine debris flows of a few cubic meters to large volcanic lahars of several cubic kilometers (Iverson *et al.*, 1998; Rickenmann, 1999; Crosta *et al.*, 2003; Yu *et al.*, 2006; Berti and Simoni, 2007; Griswold and Iverson, 2008). The ratio of horizontal runout length (L) to elevation drop (H) of a debris flow's runout path, which we refer to as the mobility index (equivalent to the inverse of the angle of reach [Heim, 1882]), is an additional measure that has been shown to increase with debris flow size (Corominas, 1996; Iverson, 1997), due mainly to the positive relationship between runout length and volume (Legros, 2002). Although the planimetric area, runout length, and mobility index scaling relationships tend to hold for event-specific debris flow inventories and regional to global debris flow data compilations, most data sets have considerable variability around the main trend. For example, the area inundated by a debris flow may vary by more than an order of magnitude for different events with the same

volume (Griswold and Iverson, 2008), while the mobility index may vary by up to a factor of four, especially for small debris flows $< 10^4$ m^3 in volume (Corominas, 1996). This unexplained variance is a source of considerable uncertainty for hazard analyses (Hürlimann *et al.*, 2008) and indicates that factors other than volume can strongly affect mobility.

Variation in debris flow mobility likely reflects properties of the debris flow itself, such as grain size distribution and water content (Iverson *et al.*, 2010; de Haas *et al.*, 2015; Hürlimann *et al.*, 2015), as well as the characteristics of the terrain through which it flows, including bed roughness and channel connectivity (e.g. Benda and Cundy, 1990; Corominas, 1996). For example, small debris flows with grain sizes that are large compared to the channel width tend to have limited runout (Crosta *et al.*, 2003), while large flows with high water contents, such as lahars (e.g. Pierson, 1985b), tend to travel farther and inundate larger areas for a given volume (Iverson *et al.*, 1998). High angle tributary junctions (Benda and Cundy, 1990; Lancaster *et al.*, 2003) and bed roughness due to engineered or natural obstacles (Hungr *et al.*, 1984; Corominas, 1996; VanDine, 1996) in the runout path also can inhibit runout. Since many debris flows occur in humid, forested, mountainous environments, the presence of large woody debris (LWD) within the flow and standing trees, stumps, or logs that affect the roughness of its path may also influence runout. The amount of LWD in a debris flow can be quite large. For example, 14 deposits with volumes of 33 to 2500 m^3 in the Oregon Coast Range contained an average of 60% LWD by volume (Lancaster *et al.*, 2003), and 15 deposits in southeast Alaskan old growth forests contained 10–35% LWD by volume (Johnson *et al.*, 2000).

During runout and deposition, both coarse sediment grains and large wood tend to congregate at the debris flow snout (Iverson, 1997; Hogan *et al.*, 1998; Lancaster *et al.*, 2003), where they often form sediment-trapping dams that determine the deposit extent (Major and Iverson, 1999). In the snout, collisional and frictional forces among individual particles are typically orders of magnitude higher than fluid forces (Iverson, 1997; Stock and Dietrich, 2006), so granular phenomena such as the creation and destruction of force chains and associated bridging or jamming effects may dominate behavior (Cates *et al.*, 1998; Furbish *et al.*, 2008; Sun *et al.*, 2010). Force chains control the behavior of dense granular flows, like a debris flow snout, because a small subset of particles supports the majority of the forces (GDR MiDi, ; Radjai *et al.*, 1998). A single particle may therefore have a large influence on the behavior of the flow as a whole. In particular, force chains are especially effective at restricting the movement of dense granular flows when the particle size is large compared to the flow dimensions (Savage and Sayed, 1984). This effect has been proposed to explain debris flow surges, wherein coarse sediment grains temporarily accumulate at a flat or constricted part of the channel and then release a surge when shear stress exceeds those grains' frictional strength (Davies, 1997; Kean *et al.*, 2013).

Although previous work has focused mainly on coarse sediment grains, large wood should behave similarly due to its large size and elongate shape. The effect of LWD on debris flow runout has been documented qualitatively and quantitatively at several sites in the forested coast ranges of western North America by comparing deposition characteristics of debris flows in old growth forests (those that have never been harvested for timber), second growth forests (those that have regrown following at least one previous harvest), and clear cuts (recently harvested forests that have not yet regrown trees). In southeast Alaska, where debris flows occur in glacially-carved valleys, deposits in old growth forests typically have snouts of LWD and travel shorter distances than those that lack LWD (Johnson *et al.*, 2000). Similarly, the presence of large standing trees in the runout path enhances deposition and can cause flows to bifurcate around isolated patches of in-place vegetation (Swanston and Marion, 1991). Compared to debris flows elsewhere, southeast Alaskan debris flows also tend to have a lower mobility index (L/H), and they deposit on steeper slopes (Johnson *et al.*, 2000). In landscapes covered by a patchwork of forest types, such as coastal British Columbia, debris flows that enter a patch of old growth forest tend to rapidly deposit within a few tens of meters, and deposition occurs on steeper slopes than elsewhere (Guthrie *et al.*, 2010). In the Oregon Coast Range, mean runout distances in clear cuts, second growth, and old growth have not been found to be significantly different, but maximum runout lengths tend to be much shorter in old growth forests (May, 2002).

In this study, we quantitatively document the effects of LWD on debris flow runout in southeast Alaska, focusing on the area near Sitka (Figure 1), which experienced at least 40 debris flows on August 18, 2015, resulting in three fatalities (Sitka GeoTask Force, 2016). Documenting runout characteristics is essential to manage future hazards in this area. Furthermore, southeast Alaska is uniquely suited to quantifying the effects of forests on runout because of the abundance of debris flows that have occurred in the extensive old growth forests that cover most of the region. We first analyze runout of 15 of the 2015 debris flows and one additional 2016 debris flow that occurred in and around Sitka based primarily on field measurements of debris flow deposit and channel geometries (Figure 1a). We then more broadly analyze debris flow mobility for an increased sample size of 1061 historic events that occurred in surrounding areas on Baranof and Chichagof Islands, and associated smaller islands, using primarily remote sensing-based geospatial data sets (Figure 1b). These analyses allow us to test two main hypotheses regarding debris flows and forests: (1) runout of debris flows in heavily forested southeast Alaska is less than runout of debris flows elsewhere, and (2) forest characteristics, such as the age, size, and spacing of trees explain variability in runout among southeast Alaskan debris flows.

Study Area

The terrain of southeast Alaska has been shaped by Pleistocene glaciations, resulting in deeply incised valleys and fjords with broad, relatively flat bottoms and steep sides (Hamilton and Thorsen, 1983; Hamilton, 1994; Kaufman and Manley, 2004). Most of the region was covered with ice caps and piedmont lobes related to the Cordilleran ice sheet and local mountain glaciers during the late Wisconsin glaciation, with those glaciers retreating rapidly by approximately 13 ka (Mann, 1986; Mann and Hamilton, 1994; Carrara *et al.*, 2007). The modern fluvial drainage network is therefore generally trellised, with short and steep low order channels joining gentler, glacial valley bottom trunk streams at high angles or flowing directly into lakes, fjords, or the open ocean. Shallow landslides that mobilize into debris flows often initiate at the heads of these low order channels in topographic hollows, and the subsequent debris flows tend to deposit on colluvial slopes, glacial valley bottoms, or beaches (Swanston and Marion, 1991; Johnson *et al.*, 2000; Gomi *et al.*, 2004).

Bedrock in southeast Alaska is varied and includes sedimentary, volcanic, and metamorphic rocks dating from the early Paleozoic to present (Gehrels and Berg, 1992). The older, pre-Cenozoic rocks have been divided into terranes that were accreted to the continental margin by the late Cretaceous, and are now bounded by major fault zones (Berg *et al.*, 1978). The north-eastern part of Chichagof Island lies within the

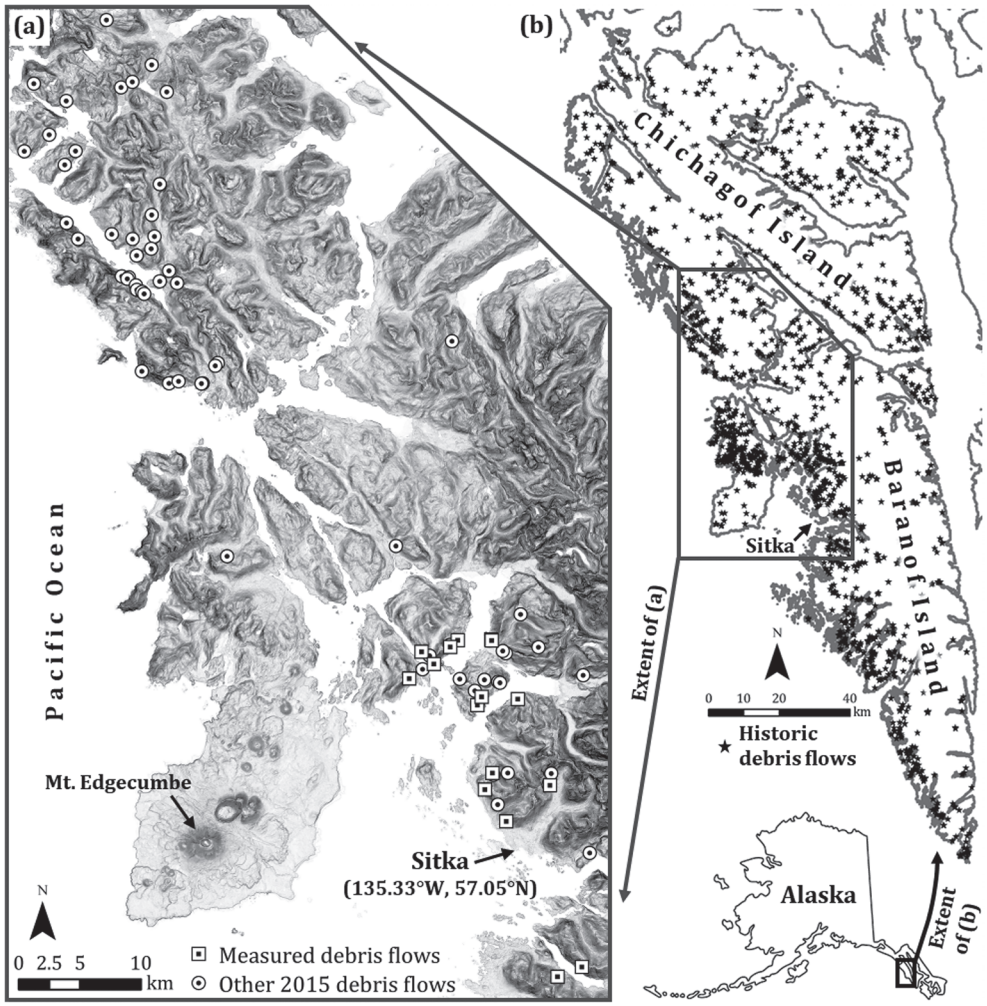

Figure 1. (a) Locations of debris flows that occurred near Sitka, Alaska on August 18, 2015 shown on a 5 m resolution slope map (circle symbols). Square symbols indicate the 16 debris flows measured as part of this study. (b) Locations of all historic debris flows on Baranof and Chichagof Islands from the Tongass National Forest database (US Department of Agriculture Forest Service, 2018).

Alexander terrain, which consists of sedimentary and volcanic rocks thought to represent intermittent volcanic arc activity on a thin fragment of continental crust (Karl, 1999). The southwestern part of Chichagof and all of Baranof Island lie within the Wrangellia and Chugach terranes, which represent an accreted Paleozoic to early Tertiary volcanic arc complex (Karl *et al.*, 2015). In the study area, Wrangellia generally consists of metasedimentary, metavolcanic, and intrusive volcanic rocks, and the Chugach terrane generally consists of sedimentary, metasedimentary, and intrusive volcanic rocks (Gehrels and Berg, 1992). Measured landslides near Sitka (Figure 1a) were located in areas with greywacke, argillite, diorite, or tonalite bedrock (Karl *et al.*, 2015).

Throughout southeast Alaska, glaciation left behind a thin layer of till over the bedrock at elevations below ~1000 m, and most debris flows have initiated below this elevation (Bishop and Stevens, 1964; Swanston, 1969, 1970; Swanston and Marion, 1991). Near Sitka, the till is directly overlain by an ~1 m thick sequence of Late Pleistocene tephras produced by the Mount Edgecumbe volcanic field on Kruzof Island, which lies 25 km to the west (Figure 1a) (Riehle *et al.*, 1992; Riehle, 1996). The lower part of the sequence consists of fine grained basaltic andesite to andesite scoria, while the upper part of the sequence consists of coarse grained rhyolitic ash and pumice. Both the lower andesitic tephras and the till are relatively dense and have low hydraulic conductivities compared to the upper rhyolitic tephras, such that groundwater tends to pond on and flow laterally along those interfaces (Johnson and Wilcock, 2002). Soils developed on those substrates can be partially or fully saturated year round, even on steep slopes (Johnson and Wilcock, 2002), and shallow landslides often develop failure planes at the bedrock–till or till–tephra interface or within the tephra (Bishop and Stevens, 1964; Swanston, 1970, 1974; Johnson *et al.*, 2000).

Modern climate at sea level in southeast Alaska is mild and maritime with generally > 2 m of annual precipitation and average high temperatures above freezing year-round (Shulski and Wendler, 2007). Intense rain storms with recurrence intervals of several years or more generally trigger shallow landslides that mobilize into debris flows in the region, and south- to west-facing slopes that are also exposed to wind during storms have higher landslide susceptibility (Gomi *et al.*, 2004; Buma & Johnson, 2015; Barth *et al.*, 2019). The August 2015 landslides in the Sitka area followed a storm with wind gusts over 40 kt and a five-hour period of rainfall with an average intensity of 1.3 to 1.5 cm h^{-1} near sea level, according to data archived on MesoWest (Horel *et al.*, 2002; Sitka GeoTask Force, 2016). Due to orographic effects, rainfall amounts and intensities were likely higher at elevations where the landslides initiated. The majority of the landslides occurred in old growth forests of dominantly Sitka spruce (*Picea sitchensis*) and western hemlock (*Tsuga heterophylla*) that are typical of the region (DellaSala *et al.*, 2011).

Methods

Sitka debris flows

In the summers of 2018 and 2019 we measured debris flow and forest characteristics in the field at 15 sites where landslides occurred as a result of the August 18, 2015 storm and one additional site where a landslide occurred in 2016 (Figure 1a). For each debris flow, we measured the deposit volume and planimetric area, the maximum inundated channel cross-section, and the depositional slope (Figure 2). To characterize the forest, we measured the size and number of trees adjacent to the debris flow runout zone. These measurements were taken to determine if the scaling relationships between runout and volume of the Sitka debris flows differed from those of debris flows elsewhere, and whether or not site specific characteristics of the forest explained differences in runout among the Sitka debris flows.

The area of the maximum inundated channel cross-section upstream of a debris flow's deposit, A, and the deposit's planimetric area, B, both have been shown to scale with flow volume as

$$A = \alpha V^{2/3}, \tag{1}$$

and

$$B = \beta V^{2/3}, \tag{2}$$

where V is the deposit volume, and α and β are dimensionless empirical constants derived from fits to measured debris flow volumes and areas (Berti and Simoni, 2007). The exponents equal to two-thirds indicate geometric scaling, such that a deposit's length, width, and depth increase in proportion to one another (Iverson *et al.*, 1998). We conducted a literature search for previously published tables of V, A, and B measurements in order to test the hypothesis that the Sitka debris flows inundated significantly different areas compared to debris flows elsewhere. Those other debris flows spanned a wide range of geologic, climatic, and ecologic settings, so that their volume–area scaling relationships should be broadly representative of debris flows in general, in contrast to those derived for the Sitka debris flows in predominantly old growth forests. For a comprehensive view of runout characteristics, we also measured total runout lengths and elevation drops from remote sensing data (satellite imagery and a 5 m resolution Interferometric Synthetic Aperture Radar [IfSAR] digital elevation model [DEM]) to determine whether or not those additional runout metrics differed from other data sets.

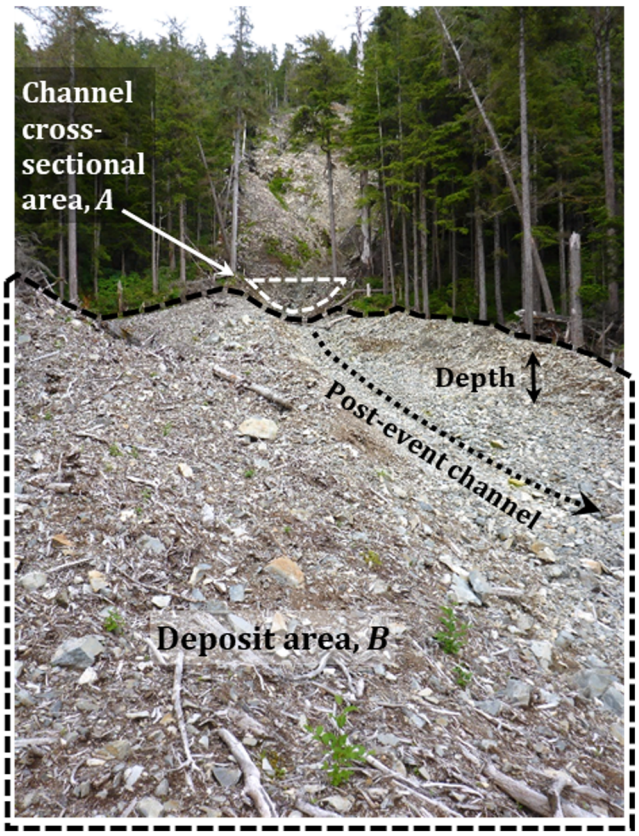

Figure 2. July 2018 photograph of the 2015 Kramer Avenue North (ID 12312, Table I) debris flow deposit and source channel, annotated to illustrate how areas and volume were measured. Deposit area continues well beyond photograph extent, and most large woody debris (LWD) has been removed from the site. Width of channel cross-section is approximately 12 m for scale. [Colour figure can be viewed at wileyonlinelibrary.com]

Since the debris flow deposits ranged in size, accessibility, and post-event fluvial modification, we employed two approaches to estimate volume (V) and planimetric area (B) in the field. The smaller flows had deposit geometries that were well approximated by either a half ellipsoid or a triangular prism, and we measured the relevant dimensions of those shapes to calculate their volumes (Crosta *et al.*, 2003; Lancaster *et al.*, 2003). Horizontal dimensions were measured directly, while depths were either measured directly where fluvial incision had subsequently cut through the deposit (e.g. Figure 2), or indirectly by surveying profiles across the deposit and linearly interpolating the underlying bed profile. For the larger and more complex deposits, all of which had been incised by post-event fluvial processes, we measured deposit depths and widths every ~10 m along a longitudinal profile and summed those segments to determine the total volume. Inundated cross sections (A) were surveyed based on high flow indicators just upslope of the apex of the debris flow deposit (Figure 2).

To estimate uncertainty on V and B, we analyzed one specific debris flow (ID 12356, Table I) using both methods described earlier, as well as an additional four variations on those approaches to capture the variability inherent in assuming that a natural, irregularly-shaped debris flow deposit can be approximated by standard geometric shapes. Specifically, we (1) multiplied the averages of our length, width, and depth measurements, which assumes a rectangular prism geometry, (2) used polynomial, rather than linear, interpolation to estimate the bed profile beneath the deposit, (3) approximated the planform geometry of the segments that were summed along the longitudinal profile as trapezoids, rather than rectangles, and (4) measured deposit area from a 1 m resolution, orthorectified satellite optical image and multiplied that by our average field-measured depth. Volumes and deposit areas calculated with these six different approaches varied by a maximum of ±20%, which we take as an estimate of the relative uncertainty for V and B. To estimate uncertainty on A, we repeated each cross-section survey three times at each site, which resulted in relative uncertainties of ±13%.

Adjacent to the deposit, we measured the diameter at breast height (DBH) of all trees $>$ 10 cm in a representative 20 m × 25 m plot. This plot size was similar to that used in previous studies (Johnson and Wilcock, 2002) and was the largest size in which it was practical to efficiently measure all trees without duplicates or omissions. For consistency with previously published forestry work, we summarized the tree data by calculating the quadratic mean diameter (QMD), defined as

Table I. Locations, volumes, and runout characteristics of Sitka debris flows

ID number[a]	UTM Easting (m)	UTM Northing (m)	V (m^3)	A (m^2)	B (m^2)	H (m)	L (m)	L/H	Deposit slope[b] (deg)
12312	477,165	6,327,810	25,390	77.2	8,281	405	698	1.7	15.5
12313	477,784	6,329,166	6,043	27.9	2,455	228	527	2.3	6.0
12336	474,943	6,340,035	79	3.9	152	61	93	1.5	15.7
12338	474,325	6,339,480	1,156	13.0	1,167	165	222	1.3	24.0
12339	472,995	6,338,098	238	9.0	240	63	100	1.6	16.0
12341	471,986	6,339,097	153	3.1	216	76	189	2.5	9.0
12343	470,999	6,336,895	789	18.8	367	105	327	3.1	8.5
12349	477,687	6,340,096	892	16.4	741	57	107	1.9	11.6
12350	477,720	6,340,025	1,221	8.3	1,112	58	112	1.9	14.5
12356	476,545	6,334,728	2,830	9.6	1,832	149	450	3.0	9.7
12358	476,891	6,335,406	858	7.3	940	81	99	1.2	25.5
12413	483,096	6,312,493	211	3.5	332	51	121	2.4	11.6
12415	485,094	6,313,280	945	8.4	990	484	730	1.5	16.5
12437	478,920	6,325,213	2,036	9.0	1,352	467	816	1.7	15.6
12646	479,854	6,335,217	1,418	12.0	915	56	152	2.7	11.0
17145	482,477	6,328,162	1,010	12.0	554	263	500	1.9	9.0

[a]Identification number in Tongass National Forest landslide database (US Department of Agriculture Forest Service, 2018).
[b]Slope measured over the full length of the debris flow deposit.

$$\mathrm{QMD} = \sqrt{\frac{\sum_{i=1}^{N} d_i^2}{N}}, \tag{3}$$

and stand density index (SDI) for uneven-aged stands, defined as

$$\mathrm{SDI} = \sum_{i=1}^{N} \left(\frac{d_i}{25.4}\right)^{1.6}, \tag{4}$$

where d_i is the diameter of each tree (in centimeters), and N is the number of trees (Curtis and Marshall, 2000; Shaw, 2000). SDI is usually calculated for all trees in 1 ha, so we multiplied the SDI of our smaller plots by 20. QMD is more commonly used than the arithmetic mean to report average tree diameters because it gives more weight to the largest trees in a plot, while SDI quantifies the relative stocking or competition in a stand and is usually uncorrelated with QMD.

Tongass National Forest historic debris flows

To expand our debris flow runout analysis to Baranof and Chichagof Islands, and associated smaller islands, we analyzed the National Forest Service database of historic landslides in the Tongass National Forest (US Department of Agriculture Forest Service, 2018). We extracted only landslides defined as debris torrents, debris avalanches, and combined debris avalanches and debris torrents, which are all generally defined as debris flows using standard landslide classification systems (Cruden and Varnes, 1996). The database included initiation points as well as polygons of the entire area affected by each landslide so that total runout lengths could be determined. Those landslides were mapped from field and aerial photograph interpretation using photographs dating from 1929 to present, and an estimate of the date of each landslide is reported in the database based on the year of the aerial photograph in which it first appeared. Dates from the most recent decade are accurate to the year on average, while older dates are accurate to within approximately a decade.

Since the volumes of landslides in the database are unknown we cannot analyze their runout using the same volume-dependent metrics as the 16 measured Sitka debris flows. Instead, we quantify runout as the mobility index, L/H. Although this metric tends to increase with debris flow size in global data sets, the data are considerably scattered for small debris flows $< 10^4$ m^3 in volume, and the presence of obstacles in the runout path, which may include trees, stumps, logs, or other roughness elements, has been found to explain much of the scatter (Corominas, 1996). Furthermore, mobility index was not correlated to volume for our data set of measured Sitka debris flows (see later), suggesting that other properties of the debris flows and conditions in their runout zones may be better predictors of mobility index. We measured H as the difference between the highest and lowest elevations in the 5 m IfSAR DEM contained in each landslide polygon, and we measured L as the maximum length of each polygon's convex hull, defined as the smallest convex polygon that completely contains the landslide polygon. Most debris flows in the database followed nearly straight runout paths, so L measured in this way closely approximated the true runout path length, although these mobility indexes should be conservative estimates for the few debris flows with more sinuous paths. The DEM was produced from 2010 to 2012, which pre-dates many recent landslides, but changes to the DEM caused by the landslides should be minimal because they are generally shallow compared to the reported vertical accuracy of 3 m.

We then analyzed the mobility indices against two geospatial data sets with information on forest characteristics. First, we extracted the forest age where each landslide occurred from a North American data set reflecting the year 2006 developed by Pan *et al*. (2011). The southeast Alaskan forest ages in that dataset were estimated from the Forest Inventory and Analysis (FIA) program of the Pacific Northwest Research Station, which estimated the average stand age of field plots by boring representative trees and counting growth rings (Barrett and Christensen, 2011). The first inventory for southeast Alaska was developed for plots spaced approximately 5 km on a hexagonal grid from 1995 to 2001, while a second inventory that revisited a subset of those plots each year was implemented beginning in 2004. Pan *et al*. (2011) interpolated the stand ages of the FIA plots to a 1 km grid and adjusted those grid cells for consistency with the 250 m spatial resolution 2003 USDA Forest Service Forest Type map (Ruefenacht *et al*., 2008). From the forest ages in the North American data set and the landslide dates in the Tongass National Forest landslide inventory we

calculated the age of the forest at the time each landslide occurred. If a landslide occurred in more than one grid cell, we used the age of the cell that contained the majority of the landslide's area.

The second forest dataset we analyzed was the size-density (SD) class model for the Tongass National Forest developed by Caouette and DeGayner (2005, 2008). Compared to the North American average stand age dataset of Pan *et al.* (2011), this data set had better spatial resolution, with an average polygon area of 0.07 km^2, and provided direct estimates of average tree size and stand density, rather than age. The SD model was produced by analyzing measured tree diameters and densities at 885 plots throughout southeast Alaska from inventories conducted in the 1980s and 1990s, and then modifying existing timber-volume maps (ESCA-Tech, 1979) based on additional soil type (hydric or non-hydric) and aspect (south- or north-facing) data. This resulted in seven SD classes that were statistically distinct in terms of QMD and SDI abbreviated SD-4H, SD-4N, SD-4S, SD-5H, SD-5 N, SD-5S, and SD-67, where H indicates hydric soils, N and S indicate north- or south-facing slopes, respectively, and the numbers 4–7 indicate previously determined timber-volume classes (ESCA-Tech, 1979). Higher numbers correspond to greater timber volumes, and class SD-67 contains both timber-volume classes 6 and 7, since statistics did not support subdividing that class according to soil type or aspect (Caouette and DeGayner, 2005). Average QMD ranges from about 40 cm to 60 cm and generally increases with timber-volume class number, while SDI ranges from about 175 to 350 and is generally higher on south-facing slopes.

We regressed the mobility index against forest age at the time of the landslide to test the hypothesis that landslides in older forests with larger trees were less mobile than those in younger forests with smaller trees. To determine whether or not average mobility index varied among SD classes, including non-forested areas, we evaluated each possible pair of SD classes and determined whether or not the mobility indices of landslides in each class had significantly different means or variances. For consistency with the development of the SD model from 1980s and 1990s inventories, we included only debris flows that occurred from 1985–present.

Results

2015 Sitka debris flows

General observations of initiation and runout

We were able to access the entire runout path of the 16 measured debris flows to visually assess the conditions of those debris flows from initiation through deposition. All but one initiation site had a distinct, arcuate head scarp ~1 m in height and was located within a subtle topographic hollow. Seeps of groundwater were present in one or more locations at the base of each head scarp, discharging onto a slicken-slided failure plane that was developed in andesitic ash, till, or dense colluvium. The landslide scars narrowed in the downslope direction and within several to tens of meters were scoured to bedrock, indicating that most of the debris flows initiated as shallow landslides before transforming into channelized flows. One debris flow (ID 12343, Table I) instead initiated in the channel below a large knickpoint, presumably due to runoff.

Bedrock exposed in the runout track was fractured with centimeter to decimeter spacing and appeared to have been incised by plucking of the uppermost blocks where pre-existing fractures were favorably oriented. In the argillite bedrock, the margins of the runout channels also had a popcorn texture indicative of wet-dry weathering. The debris flow tracks in the argillite were contained within relatively smooth and well-defined channels compared to those in the greywacke and diorite bedrock, where the tracks followed more broadly concave valleys, often with a small, meter-scale channel incised near the center. Localized clusters of deposition were also present in and at the lateral margins of these channels upstream of large trees, boulders, or other roughness elements and on relatively flat reaches.

The transition from the runout track to the debris flow deposit was typically abrupt and occurred at a break in slope where the flow encountered a valley bottom, trunk stream, colluvial slope, or beach (Figures 3a and 3b). Most of the deposits contained abundant woody debris, which often formed lateral levees and a snout at the downstream end, with finer grained material backed-up behind it (Figures 3c–3f).

Quantitative runout analysis

Volumes of the 16 measured debris flow deposits ranged from 80 to 25 000 m^3 (Table I), with half of the deposits having a volume of about 1000 m^3 (middle 50th percentile 789 to 1418 m^3). Maximum inundated channel cross-sections ranged from 3 to 77 m^2, while planimetric areas of the deposits ranged from 150 to 8300 m^2. Both data sets were well-fit by Equations (1) and (2), which we determined by log-transforming the data and using linear least squares regression with a fixed regression slope of two-thirds (Figure 4) (Berti and Simoni, 2007; Griswold and Iverson, 2008). For the channel cross-section data, $\alpha = 0.11$ (0.08–0.14, 95% confidence interval) explained 64% of the variance, and for the deposit area data, $\beta = 8.0$ (7.0–9.2) explained 94% of the variance.

To test the hypotheses that the Sitka debris flows inundated significantly different planform and channel cross-sectional areas for a given volume, we compared α and β of those 16 debris flows to a global compilation taken from the literature. The compilation consisted only of non-volcanic debris flows, and included a global database (Griswold and Iverson, 2008), debris flows in the European Alps (Berti and Simoni, 2007; D'Agostino *et al.*, 2010; Scheidl and Rickenmann, 2010; Simoni *et al.*, 2011), and in Arizona (Webb *et al.*, 2008). Debris flows in this compilation had similar sizes to the Sitka debris flows (Figure 4), with a median volume of 10^4 m^3, and spanned a wide range of initiation mechanisms and geologic, climatic, and ecological settings which we assume are broadly representative of debris flows in general. This literature review yielded 90 debris flows for which both V and A were known and 69 debris flows for which both V and B were known, where B was defined as the deposit area. We then tested whether or not the regression intercepts of the Sitka data were significantly different from those of the global data at a 95% confidence level. For the global data, the best fit parameters were $\alpha = 0.07$ (0.05–0.08), which explained 59% of the variance, and $\beta = 26.0$ (22–31), which explained 69% of the variance. The best-fit α for the Sitka data was higher than that of the global data, but the difference was not statistically significant. However, the best-fit β for the Sitka data was significantly lower than that of the global data, indicating that the Sitka debris flow deposits inundated about one-third of the planimetric area predicted by the fit to the global data set for a given volume.

Maximum horizontal runout lengths of the Sitka debris flows ranged from 93 to 730 m and generally increased with volume (Table I, Figure 5a). We analyzed this horizontal runout in two ways to enable comparison to previously published data: (1) maximum runout length plotted against the product of volume and drop height (VH), which is a proxy for potential energy (Rickenmann, 1999), and (2) the mobility index. Runout

Figure 3. Maps and photographs illustrating typical characteristics of debris flow deposits. (a) Orthorectified aerial photograph and (b) LiDAR-derived slope map of debris flow ID 12313 with location of the upslope end of the deposit annotated to illustrate deposition beginning at a break in slope below a steep valley wall. (c-f) Photographs illustrating effects of large woody debris (LWD) that likely restricted runout, with black arrows indicating flow direction and approximate scale bars. (c) ID 12343. View of entire deposit from top of left-hand channel bank showing a rim of LWD that trapped sediment and set the extent of the ~25 m wide deposit. (d) ID 12312. Detail of a log and root ball that were wedged against an ~1 m diameter standing tree, retaining sediment along the edge of the deposit. (e) ID 12313. View looking upstream at the end of the deposit snout, which consisted predominantly of LWD. (f) ID 12313. View looking down at ~20 m wide deposit from top of left-hand channel bank showing sediment retained behind rim of LWD in a trunk stream valley. [Colour figure can be viewed at wileyonlinelibrary.com]

lengths of the 16 measured Sitka debris flows were positively correlated to *VH*, as determined by linear regression of the log-transformed variables (Figure 5a), but were lower than expected compared to other debris flows (Rickenmann, 1999). The relationship from Rickenmann (1999) was based on a qualitative fit that assumed geometric scaling to debris flow data from primarily the Swiss Alps (n = 140), with additional data from the Canadian Cordillera (n = 8), Japan (n = 6), North and South American Cordilleran volcanoes (n = 3), and the US Geologic Survey debris flow flume (n = 13). The Swiss debris flows that dominate the relationship primarily initiated in sparsely-vegetated periglacial environments and flowed down channels through a mix of forested and agricultural land (Rickenmann and Zimmermann, 1993). Since the fit to that data was not derived statistically, we cannot determine whether the Sitka data are significantly different, but we note that the measured Sitka debris flows traveled just 20–94% of the horizontal distance predicted from the Rickenmann (1999) data set. The mobility indices of the Sitka debris flows ranged from 1.4 to 3.1 (Table I), and were not significantly correlated with volume. However, this range of values is generally at the lower end of the range of approximately 1.3 to 6 documented for debris flows of similar volumes elsewhere (Corominas, 1996; Rickenmann, 2005).

Although inundated areas and runout lengths were significantly correlated with debris flow volume or potential energy, respectively, there was still considerable variability from these main trends for individual debris flows. We sought to explain this variability by regressing the relative deviation from the trend against site-specific forest characteristics (QMD and SDI) and the degree of channelization of the runout path, defined as the channel depth to width ratio upstream of the

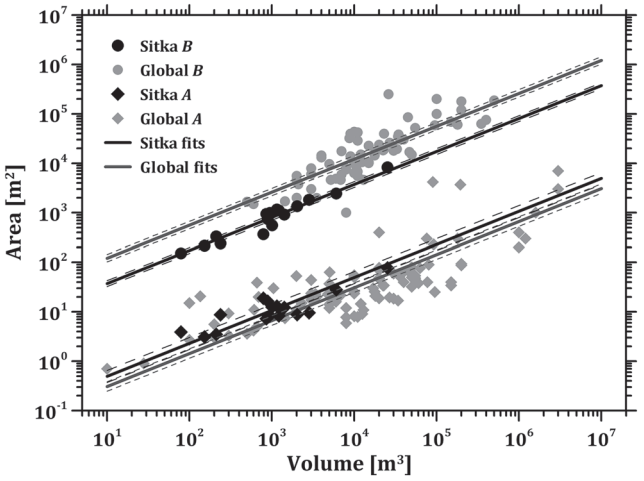

Figure 4. Maximum inundated channel cross-section area (*A*, diamonds) and debris flow deposit planimetric area (*B*, circles) versus debris flow volume (*V*) for the measured Sitka debris flows (black) and a global compilation (gray). Solid lines are best-fit linear regressions of log-transformed Equations (1) and (2), and dashed lines are 95% confidence intervals (CI) on the log-transformed values of α and β. The lower 95% CI for the Sitka *V* versus *A* fit overlies the upper 95% CI of the global *V* versus *A* fit at the scale of the figure.

deposit. The relative deviations of deposit area and channel cross-section area were not significantly correlated to either of the forest metrics or to the degree of channelization. The relative deviation of runout length was not correlated to forest characteristics, but did increase significantly (regression slope of 2.5 [0.9–4.2]) with the degree of channelization (Figure 5b). This suggests that for a given volume, the more channelized flows that occurred in the argillite bedrock were able to travel farther than the less channelized ones in the greywacke, diorite, or tonalite bedrock, even though deposit areas were similar.

Tongass National Forest historic landslide mobility

Since we found no relationship between runout and forest characteristics of the 16 measured Sitka debris flows, we expanded our analysis to 1061 historic debris flows on Baranof and Chichagof Islands for an increased sample size and broader representation of different debris flow triggering events and forest characteristics. Volume is unknown for these debris flows, so we used mobility index to quantify their runout.

The mobility indices of the historic debris flows averaged 2.2 ± 1.4 (mean ± standard deviation) and were log-normally distributed. Because of the relatively large scatter in the mobility indices, we applied three different regressions to test whether or not there was a significant relationship between mobility index and forest age or debris flow area. A linear fit was defined by applying linear regression to the untransformed data, an exponential fit was defined by applying linear regression after log-transforming the mobility index, and a power law fit was defined by applying linear regression after log-transforming both mobility index and the independent variable (forest age or debris flow area) (Table II). Although none of the fits explained a high proportion of the variance (r^2 ranged from 0.001 to 0.07), mobility index was significantly (> 95% confidence) and negatively correlated with forest age, which ranged from 0 to 416 years, for all three fit types (Figure 6). The fits predicted a mobility index of 2.3 to 2.5 for the youngest forests,

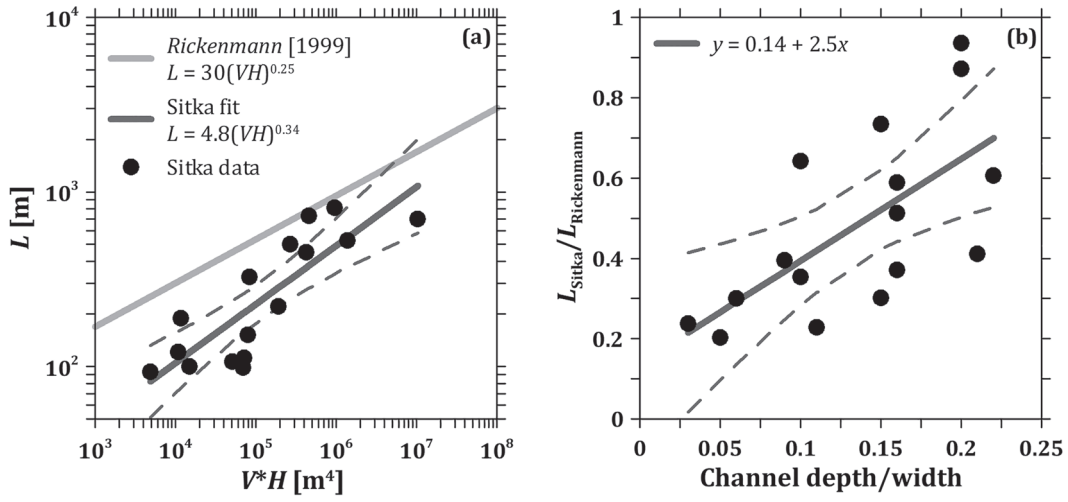

Figure 5. (a) Maximum runout length (*L*) versus the product of debris flow volume and maximum elevation drop (*VH*) for the measured Sitka debris flows, with theoretical prediction from Rickenmann (1999) for comparison. (b) Ratio of measured maximum runout length to that predicted in Rickenmann (1999) versus the depth to width ratio of the channel above the debris flow deposit. Dashed lines are 95% confidence intervals on the fits in both (a) and (b).

Table II. Summary of mobility index regression slopes

Fit type	Mobility index versus forest age		Mobility index versus landslide area	
	Regression slope[a] (95% confidence interval)	r^2	Regression slope[a] (95% confidence interval)	r^2
Linear	**-0.003** (-0.004, -0.002)	0.04	**-4.8×10^{-6}** (-9.5×10^{-6}, -5.1×10^{-8})	0.004
Exponential	**-0.0004** (-0.0005, -0.0003)	0.07	-3.3×10^{-7} (-9.3×10^{-7}, 2.6×10^{-7})	0.001
Power law	**-0.06** (-0.07, -0.04)	0.06	**-0.05** (-0.07, -0.03)	0.02

[a]Regression slopes that differ significantly from zero at the 95% confidence level are shown in bold.

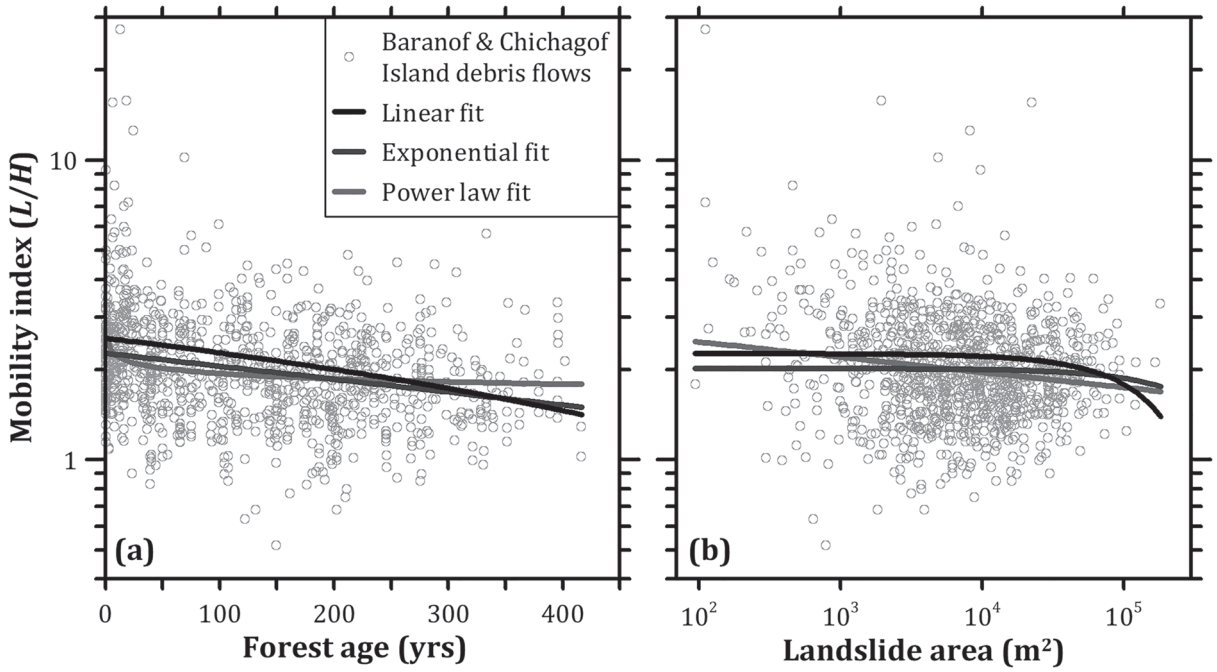

Figure 6. (a) Mobility index versus forest age, and (b) versus landslide area for all mapped historic debris flows on Baranof and Chichagof Islands (points) and linear, exponential, and power law fits (lines) (Table II).

which decreased to 1.4–1.8 for the oldest forests. Regressions of mobility index against debris flow area showed either no significant trend (exponential fit), or a significant negative trend that was weak compared to the corresponding regression against forest age (linear and power law fits) (Table II). This demonstrates that forest age is a better predictor of debris flow mobility index than debris flow size for the data set.

Debris flows from 1985 to present occurred in six of the seven SD classes identified in Caouette and DeGayner (2005, 2008), excluding SD-5H, as well as in non-forested (NF) areas. Additionally, we grouped all SD classes into one class defined as old growth (OG) to directly compare to the NF class. The mean mobility indices were not significantly different for any pair of SD classes, as determined by *t*-tests performed on the log-transformed data. However, mobility indices of 10 pairs of SD classes had significantly different variances, as determined by the *F*-test of equality of variances on the log-transformed data (Table III). Overall, the variance of the mobility index of debris flows occurring in OG was significantly less than that of debris flows in NF, indicating that those debris flows with high mobility indices that would cause the distribution to have high variance are less common in OG. More specifically, the variance of mobility index in the SD-67 group was less than in all but one of the other SD classes. The SD-67 class had the largest trees of all classes with an average QMD of approximately 55 cm. Similarly, the variances of the mobility index in all but two of the SD classes were less than in the NF class. The exceptions were SD-4H and SD-5N, which showed no significant difference in variance and had low sample sizes of 11 and 10 debris flows, respectively. Class SD-4H also contained the smallest trees of all classes with a QMD of approximately 40 cm. The only other significant difference in variance in mobility index was that debris flows in SD-4 N, where QMD was approximately 47 cm, were less mobile than those in SD-4H. In general, the analysis of mobility index with respect to forest class showed that debris flows tended to be less mobile in forests with a larger QMD, and that this effect was especially pronounced in the most mature old growth forests (SD-67).

Discussion

Results of this study demonstrate that the Sitka debris flows were significantly less mobile than debris flows elsewhere, and more generally that the mobility of debris flows in

Table III. The *P*-values of *F*-tests[a] of equality of variances on mobility indices for each pair of size-density (SD) classes

SD classes from Caouette and DeGayner (2005)							
OG[b] (*n* = 251)	SD-4H (*n* = 12)	SD-4N (*n* = 29)	SD-4S (*n* = 132)	SD-5N (*n* = 12)	SD-5S (*n* = 59)	SD-67 (*n* = 7)	
-8.4×10^{-4}	-0.096	**-0.009**	**-0.002**	-0.061	**-0.038**	**-0.001**	NF[c] (*n* = 42)
		-0.027	-0.065	-0.093	-0.165	**-0.002**	SD-4H
			0.250	0.863	0.157	-0.051	SD-4N
				-0.491	0.543	**-0.011**	SD-4S
					0.358	**-0.048**	SD-5N
						-0.008	SD-5S

[a]Significant differences are shown in bold typeface, and a negative sign indicates that the SD class on the top of the table was less mobile than the SD class on the right side of the table.
[b]Old growth (OG) category includes all listed SD classes.
[c]NF, non-forested.

southeast Alaska was lower in older forests with larger trees. We now consider mechanisms that potentially contributed to that reduced mobility by focusing on the processes responsible for debris flow deposition. The extent of a debris flow deposit is set by the friction-dominated, coarse-grained snout and lateral levees, which deposit first, forming a dam that resists momentum of the following fluidized, fine-grained debris flow tail (Suwa and Okuda, 1983; Pierson, 1985a; Major and Iverson, 1999; Major, 2000). Higher water content, proportion of mud-sized sediment, and degree of lateral confinement have been shown to increase runout primarily by affecting the fluidized tail (Iverson *et al.*, 2010), while increases in grain size, tributary junction angles (Benda and Cundy, 1990; Lancaster *et al.*, 2003), and obstacles in the runout zone (Corominas, 1996) restrict runout primarily by affecting the friction-dominated snout.

We do not expect processes that primarily affect the fluidized tail to be much different in southeast Alaskan debris flows than elsewhere. First, water content is likely comparable to that of other similarly-sized debris flows because precipitation events that trigger debris flows in southeast Alaska have typically high intensities and durations. For example, the 2015 storm in Sitka had a five hour duration with an average rainfall intensity of 1.3 cm h^{-1} measured at the Sitka Airport at sea level on an island in Sitka Sound and 1.5 cm h^{-1} measured at the Sitka Geomagnetic Observatory, located ~1 km inland at an elevation of 20 m above sea level, according to data archived on MesoWest (Horel *et al.*, 2002). Peak rainfall intensities recorded at the Geomagnetic Observatory were 2.1 cm h^{-1}, 6.1 mm in 15 minutes, and 2.3 mm in five minutes. Other documented storms in southeast Alaska that have triggered debris flows had intensities of 0.5 to 0.6 cm h^{-1} for durations of 24 hours (Swanston, 1969, 1970; Gomi *et al.*, 2004) or total precipitation amounts of 20.9 cm (Johnson *et al.*, 2000). These precipitation amounts are consistent with thresholds that triggered debris flows in a wide variety of locations (Caine, 1980; Guzzetti *et al.*, 2008; Baum and Godt, 2010). Second, the soils in the Sitka area involved in the debris flows are mostly silty sands and silty gravels (Unified Soil Classification System classes SM and GM, respectively), which contain more than 12% fines, defined as grains less than 0.074 mm in diameter (Schroeder, 1983; Ping *et al.*, 1989; Golder Associates, 2001, 2008). In large-scale debris flow flume experiments, a 7% proportion of fines, defined as less than 0.0625 mm in diameter, was sufficient to generate muddy debris flows with longer runout compared to debris flows that lacked fines (Iverson *et al.*, 2010). Last, lateral confinement had a secondary effect on runout length of the Sitka debris flows (Figure 5b), but even those flows in the most well-defined channels ran out much less than expected based on data sets from outside southeast Alaska, in terms of both horizontal runout length and deposit area (Figures 4 and 5a).

Instead, we interpret that in heavily-forested southeast Alaska processes involving LWD in the debris flow snout and its interactions with standing trees, stumps, and logs in the runout path caused the lower than expected mobility. Granular phenomena controlled by frictional forces acting among particles in the debris flow snout, such as force chains, likely determine the extent of debris flow deposition in general (Major and Iverson, 1999), and in southeast Alaska, we expect the density, size, and shape of LWD in debris flows to make it even more effective than coarse sediment alone at restricting mobility. Since wood is less dense than sediment, buoyant forces should more easily move it to the surface of the flow during runout, where it can then move to the flow front and be retained at the snout by processes such as kinetic sieving (Middleton, 1970; Rosato *et al.*, 1987; Vallance and Savage, 2000). The LWD entrained by debris flows in old growth stands that we visited in the field was typically on the order of 0.5 m in diameter and several to tens of meters in length, which was much larger than the coarsest sediment grains of cobble to boulder size. Average deposit depths ranged from 0.5 to 3 m (Table I) and were therefore similar to the dimensions of the entrained LWD, a condition that facilitates jamming of debris flow snouts (Davies, 1997). Furthermore, the elongate shape of logs meant that they were often long enough to span the entire channel cross-section as well as the gaps between standing trees in the runout path. We frequently observed large wood levees and snouts that were wedged against standing trees, forming dams that withheld fine-grained deposits of primarily sediment, suggesting that the elongate shape of LWD was especially effective at resisting the momentum of the debris flow tail and constraining runout extent (Figure 3).

Although the abundance of LWD in the Sitka debris flows was the most clearly visible mechanism for restricting runout there, similar jamming effects facilitated by force chains should occur more generally when the size of sediment or wood in a debris flow snout is large compared to the flow dimensions. This condition may be met by sediment alone in some of the smallest debris flows, as reflected by the scaling of deposit area with volume (Equation (2)). For example, small debris flows of order 10^1 to 10^5 m^3 in volume originating in rocky, sparsely vegetated talus slopes in the Italian Alps have a coefficient β of 6.2, which was attributed to the fictional, granular nature of those debris flows (Crosta *et al.*, 2003). That value is comparable to β = 8.0 determined for the Sitka data set, despite the majority of those flows having volumes orders of magnitude less than the debris flows in Sitka. For debris flows with volumes of order 10^3 to 10^4 m^3, like those in Sitka, and larger, it becomes increasingly rare to find sediment grains that are large compared to the flow dimensions. We suspect this is why numerous data sets of debris flow deposit areas and volumes have a larger coefficient β of 17 to 45 (Crosta and Dal Negro, 2003; Berti and Simoni, 2007; D'Agostino *et al.*, 2010; Scheidl and Rickenmann, 2010; Simoni *et al.*, 2011). The largest lahars with volumes of order 10^5 to 10^9 m^3 typically have even larger β values of around 200, although in many studies this area includes the runout zone in addition to the deposit (Iverson *et al.*, 1998). Overall, the coefficient β appears to be smallest for the smallest debris flows, and we interpret that granular processes acting among the large wood, if present, or sediment grains are the primary mechanism that causes these deeper, less extensive deposits.

The limited runout of debris flows in southeast Alaska, which we attribute mainly to the heavily forested environment, suggests that both empirical hazard assessments and physics-based numerical modeling of debris flows could be improved by explicitly incorporating LWD. For accurate empirical hazard analysis, the distribution of vegetation in a landscape, in addition to the geologic conditions, should be considered when developing site-specific scaling relationships between debris flow size and runout. Using generic scaling relationships that may have been developed for debris flows in different environmental settings may severely over or under predict runout. Current physics-based numerical models of debris flow runout typically assume depth-averaged properties of a two-phase mixture of sediment and fluid (e.g. George and Iverson, 2014; Iverson and George, 2014) or simulate coupled sediment and fluid motion (e.g. Pudasaini, 2012). Most models therefore by design do not capture potential effects of LWD, but could be modified to do so by explicitly including wood as an additional solid phase with lower density, more elongate shape, and larger size compared to sediment.

Conclusions

In this study, we used field and remote sensing data to quantify the effects of forest structure on debris flow mobility in southeast Alaska. We measured volumes and runout characteristics of 16 debris flows, 15 of which mobilized from shallow landslides near Sitka during an intense rainfall event on August 18, 2015, and compared their behavior to a global compilation of debris flow characteristics to determine whether the Sitka debris flows were more or less mobile than typically observed. We then analyzed the mobility of 1061 historic debris flows that occurred in a larger region around Sitka, including Baranof and Chichagof Islands, with respect to forest characteristics to determine if mobility was related to average tree age, size, and density.

The 2015 Sitka debris flows were significantly less mobile than debris flows elsewhere, as quantified by the scaling between deposit area and volume. The Sitka debris flow deposits inundated 8.0 times their volume raised to the two-thirds power, while debris flows of similar size from a global compilation inundated 26 times their volume to the two-thirds power. This indicates that the Sitka debris flows formed relatively thick deposits that covered just 31% of the area that would be predicted by scaling relationships defined for other regions. Runout lengths of the 2015 Sitka debris flows were similarly restricted, traveling an average of 48% of the total horizontal distance compared to debris flows from other locations. Debris flows that ran out through deep, narrow channels were the most mobile, all else being equal. Last, the Sitka debris flows deposited on slopes of 6° to 26° and had mobility indices, defined as the ratio of horizontal runout to vertical elevation change, from 1.2 to 3, which both indicate low mobility compared to debris flows elsewhere.

Historic debris flows on Chichagof and Baranof Islands had a similarly small average mobility index of 2.2, which decreased significantly from about 2.3–2.5 to 1.4–1.8 as average forest age increased from 0 to 416 years. Mobility index either weakly negatively correlated or did not correlate with debris flow area, implying that the age of the trees where a debris flow occurred was the primary control on its mobility. Analysis of mobility index with respect to a forest stand SD model further showed that the oldest forest class with the largest diameter trees contained debris flows that were significantly less mobile than all but one of the other, younger forest classes. Overall, these results implied that average tree size, which is reflected in the average forest age, was the predominant control on debris flow mobility.

We interpreted that granular phenomena, such as jamming due to force chains, acting among large wood in the debris flow snout and in the runout path were the main processes responsible for the observed limited runout. Specifically, the large size, elongate shape, and low density of wood mobilized by the debris flows was likely more effective than coarse sediment alone at restricting runout, especially considering the spacing of standing trees in the deposition zones. These results highlight the importance of taking local conditions, including forest properties, into account when conducting debris flow runout hazard analyses. Using an empirical runout relationship derived for one region may result in a many-fold over or under prediction of runout if applied to another region. Furthermore, over geologic time, our results suggest that landslides and vegetation may co-evolve to control the routing of sediment and wood from high elevation sources to low elevation sinks throughout mountainous landscapes.

Acknowledgements—The authors thank the Associate Editor and two anonymous reviewers for constructive criticism that improved the manuscript. The authors thank the Sitka Sound Science Center for assisting with fieldwork. AMB was supported by NSF EAR-1711986 and BB was supported by NSF EAR-1711974.

Conflict of Interest Statement

The authors have no conflicts of interest to declare.

Co-author Justification

Bryce Vascik was added as co-author because he collected and analyzed data that was added to the manuscript during the revision process.

Data Availability Statement

The data that support the findings of this study are openly available in the USDA Forest Service Geodata Clearing House at https://data.fs.usda.gov/geodata/ (Tongass National Forest Landslide Inventory), in the southeast Alaska GIS Library at http://seakgis.alaska.edu/ (Tongass National Forest Size-Density Model), in the Oak Ridge National Laboratory Distributed Active Archive Center at https://doi.org/10.3334/ORNLDAAC/1096 (North American Forest Ages), in the USGS Earth Resources Observation and Science (EROS) Center at https://www.usgs.gov/centers/eros (IfSAR Digital Elevation Model), and in MesoWest at https://mesowest.utah.edu/ (Precipitation Data).

References

Anderson SW, Anderson SP, Anderson RS. 2015. Exhumation by debris flows in the 2013 Colorado Front Range storm. *Geology* **43**: 391–394. https://doi.org/10.1130/g36507.1.

Barrett TM, Christensen GA. 2011. *Forests of Southeast and South-central Alaska, 2004–2008: Five-year Forest Inventory and Analysis Report, General Technical Report PNW-GTR-835*. US Department of Agriculture, Forest Service, Pacific Northwest Research Station: Portland, OR.

Barth S, Geertsema M, Bevington AR, Bird AL, Clague JJ, Millard T, Bobrowsky PT, Hasler A, Liu H. 2019. Landslide response to the 27 October 2012 earthquake (M_W 7.8), southern Haida Gwaii, British Columbia, Canada. *Landslides*: 1–10. https://doi.org/10.1007/s10346-019-01292-7.

Baum RL, Godt JW. 2010. Early warning of rainfall-induced shallow landslides and debris flows in the USA. *Landslides* **7**: 259–272. https://doi.org/10.1007/s10346-009-0177-0.

Benda LE, Cundy TW. 1990. Predicting deposition of debris flows in mountain channels. *Canadian Geotechnical Journal* **27**: 409–417. https://doi.org/10.1139/t90-057.

Benda LE, Dunne T. 1997. Stochastic forcing of sediment supply to channel networks from landsliding and debris flow. *Water Resources Research* **33**: 2849–2863. https://doi.org/10.1029/97WR02388.

Berg HC, Jones DL, Coney PJ. 1978. Map Showing pre-Cenozoic Tectonostratigraphic Terranes of Southeastern Alaska and Adjacent Areas, Scale 1:1,000,000, US Geological Survey Open-File Report 78-1085. US Geological Survey: Reston, VA, https://doi.org/10.3133/ofr781085.

Berti M, Simoni A. 2007. Prediction of debris flow inundation areas using empirical mobility relationships. *Geomorphology* **90**: 144–161. https://doi.org/10.1016/j.geomorph.2007.01.014.

Bishop DM, Stevens ME. 1964. Landslides on Logged Areas in Southeast Alaska, USDA Forest Service Research Paper NOR-1. US Forest Service: Washington, DC.

Buma B, Johnson AC. 2015. The role of windstorm exposure and yellow cedar decline on landslide susceptibility in southeast Alaskan

temperate rainforests. *Geomorphology* **228**: 504–511. https://doi.org/10.1016/j.geomorph.2014.10.014.

Caine N. 1980. The rainfall intensity – duration control of shallow landslides and debris flows. *Geografiska Annaler Series A – Physical Geography* **62**: 23–27. https://doi.org/10.2307/520449.

Caouette JP, DeGayner EJ. 2005. Predictive mapping for tree sizes and densities in southeast Alaska. *Landscape and Urban Planning* **72**: 49–63. https://doi.org/10.1016/j.landurbplan.2004.09.012.

Caouette JP, DeGayner EJ. 2008. Broad-scale classification and mapping of tree size and density attributes in productive old-growth forests in Southeast Alaska's Tongass National Forest. *Western Journal of Applied Forestry* **23**: 106–112. https://doi.org/10.1093/wjaf/23.2.106.

Carrara PE, Ager TA, Baichtal JF. 2007. Possible refugia in the Alexander Archipelago of southeastern Alaska during the late Wisconsin glaciation. *Canadian Journal of Earth Sciences* **44**: 229–244. https://doi.org/10.1139/e06-081.

Cates ME, Wittmer JP, Bouchaud JP, Claudin P. 1998. Jamming, force chains, and fragile matter. *Physical Review Letters* **81**: 1841–1844. https://doi.org/10.1103/PhysRevLett.81.1841.

Corominas J. 1996. The angle of reach as a mobility index for small and large landslides. *Canadian Geotechnical Journal* **33**: 260–271. https://doi.org/10.1139/t96-005.

Crosta G, Cucchiaro S, Frattini P. 2003. Validation of semi-empirical relationships for the definition of debris-flow behavior in granular materials. In *In Proceedings of the Third International Conference on Debris-flow Hazards Mitigation: Mechanics, Prediction and Assessment*. MillPress: Rotterdam: Davos, Switzerland; 821–831.

Crosta GB, Dal Negro, P. 2003. Observations and modelling of soil slip-debris flow initiation processes in pyroclastic deposits: the Sarno 1998 event. *Natural Hazards and Earth System Sciences* **3**: 53–69. https://doi.org/10.5194/nhess-3-53-2003.

Cruden DM, Varnes DJ. 1996. Landslide types and processes. In *Landslides: Investigation and Mitigation, Special Report 247*, Turner AK, Schuster RL (eds). National Academy Press: Washington, DC.

Curtis RO, Marshall DD. 2000. Why quadratic mean diameter? *Western Journal of Applied Forestry* **15**: 137–139. https://doi.org/10.1093/wjaf/15.3.137.

D'Agostino V, Cesca M, Marchi L. 2010. Field and laboratory investigations of runout distances of debris flows in the Dolomites (Eastern Italian Alps). *Geomorphology* **115**: 294–304. https://doi.org/10.1016/j.geomorph.2009.06.032.

Davies TR. 1997. Large and small debris flows – occurrence and behaviour. In *Recent Developments on Debris Flows*, Armanini A, Michiue M (eds). Springer Verlag: Berlin.

de Haas T, Braat L, Leuven JR, Lokhorst IR, Kleinhans MG. 2015. Effects of debris flow composition on runout, depositional mechanisms, and deposit morphology in laboratory experiments. *Journal of Geophysical Research: Earth Surface* **120**: 1949–1972. https://doi.org/10.1002/2015JF003525.

DellaSala DA, Moola F, Alaback P, Paquet PC, Schoen JW, Noss RF. 2011. Temperate and boreal rainforests of the Pacific Coast of North America. In *Temperate and Boreal Rainforests of the World: Ecology and Conservation*, DellaSala DA (ed). Springer Verlag: Berlin; 42–81.

Dowling CA, Santi PM. 2014. Debris flows and their toll on human life: a global analysis of debris-flow fatalities from 1950 to 2011. *Natural Hazards* **71**: 203–227. https://doi.org/10.1007/s11069-013-0907-4.

Eaton LS, Morgan BA, Kochel RC, Howard AD. 2003. Role of debris flows in long-term landscape denudation in the central Appalachians of Virginia. *Geology* **31**: 339–342. https://doi.org/10.1130/0091-7613(2003)031<0339:RODFIL>2.0.CO;2.AK.

ESCA-Tech Corporation. 1979. General Services Administration, Standard Form 33. On file with: USDA Forest Service, Alaska Region, P. O. Box 21628, Juneau, AK 99802.

Furbish DJ, Schmeeckle MW, Roering JJ. 2008. Thermal and force-chain effects in an experimental, sloping granular shear flow. *Earth Surface Processes and Landforms* **33**: 2108–2117. https://doi.org/10.1002/esp.1655.

GDR MiDi. On dense granular flows. *European Physical Journal E* **14**: 341–365. https://doi.org/10.1140/epje/i2003-10153-0

Gehrels GE, Berg HC. 1992. *Geologic Map of Southeastern Alaska*, US Geological Survey Open-File Report 84-886. US Geological Survey: Reston, VA.

George DL, Iverson RM. 2014. A depth-averaged debris-flow model that includes the effects of evolving dilatancy. II. Numerical predictions and experimental tests. *Proceedings of the Royal Society A: Mathematical, Physical and Engineering Sciences* **470**(2170): 20130820. https://doi.org/10.1098/rspa.2013.0820.

Golder Associates. 2001. *Final Report to USKH, Inc. and United States Forest Service for Geotechnical Investigation Harbor Mountain Road Sitka, Alaska*. Golder Associates: Toronto.

Golder Associates. 2008. *Final Report on Geotechnical Investigation Whitcomb Heights Subdivision, Sitka, Alaska*. Golder Associates: Toronto.

Gomi T, Sidle RC, Swanston DN. 2004. Hydrogeomorphic linkages of sediment transport in headwater streams, Maybeso Experimental Forest, southeast Alaska. *Hydrological Processes* **18**: 667–683. https://doi.org/10.1002/hyp.1366.

Griswold JP, Iverson RM. 2008. Mobility Statistics and Automated Hazard Mapping for Debris Flows and Rock Avalanches. US Geological Survey Scientific Investigations Report, 2007–5276. US Geological Survey: Reston, VA.

Guthrie RH, Hockin A, Colquhoun L, Nagy T, Evans SG, Ayles C. 2010. An examination of controls on debris flow mobility: evidence from coastal British Columbia. *Geomorphology* **114**: 601–613. https://doi.org/10.1016/j.geomorph.2009.09.021.

Guzzetti F, Peruccacci S, Rossi M, Stark CP. 2008. The rainfall intensity–duration control of shallow landslides and debris flows: an update. *Landslides* **5**: 3–17. https://doi.org/10.1007/s10346-007-0112-1.

Hamilton TD. 1994. Late Cenozoic glaciation of Alaska. In *The Geology of Alaska*, Plafker G, Berg HC (eds). The Geological Society of America: Boulder, CO.

Hamilton TD, Thorsen RM. 1983. The Cordilleran Ice Sheet in Alaska. In *Late Quaternary Environments of the United States, 1, The Late Pleistocene*, Porter SC (ed). University of Minnesota Press: Minneapolis, MN; 38–52.

Heim A. 1882. Der bergsturz von Elm. *Zeitschrift der Deutschen Geologischen Gesellschaft* **34**: 74–115.

Hogan D, Bird S, Hassan M. 1998. Spatial and temporal evolution of small coastal gravel-bed streams: influence of forest management on channel morphology and fish habitats. In *Gravel-bed Rivers in the Environment*, Klingeman PC, Beschta RL, Komar PD, Bradley JB (eds). Water Resources Publications: Highlands Ranch, CO; 365–392.

Horel J, Splitt M, Dunn L, Pechmann J, White B, Ciliberti C, Lazarus S, Slemmer J, Zaff D, Burks J. 2002. Mesowest: cooperative mesonets in the western United States. *Bulletin of the American Meteorological Society* **83**(2): 211–226. https://doi.org/10.1175/1520-0477(2002)083<0211:MCMITW>2.3.CO;2.

Hungr O, Morgan G, Kellerhals R. 1984. Quantitative analysis of debris torrent hazards for design of remedial measures. *Canadian Geotechnical Journal* **21**: 663–677. https://doi.org/10.1139/t84-073.

Hürlimann M, Rickenmann D, Medina V, Bateman A. 2008. Evaluation of approaches to calculate debris-flow parameters for hazard assessment. *Engineering Geology* **102**: 152–163. https://doi.org/10.1016/j.enggeo.2008.03.012.

Hürlimann M, McArdell BW, Rickli C. 2015. Field and laboratory analysis of the runout characteristics of hillslope debris flows in Switzerland. *Geomorphology* **232**: 20–32. https://doi.org/10.1016/j.geomorph.2014.11.030.

Iverson RM. 1997. The physics of debris flows. *Reviews of Geophysics* **35**: 245–296. https://doi.org/10.1029/97rg00426.

Iverson RM, George DL. 2014. A depth-averaged debris-flow model that includes the effects of evolving dilatancy. I. Physical basis. *Proceedings of the Royal Society A: Mathematical, Physical and Engineering Sciences* **470**(2170): 20130819. https://doi.org/10.1098/rspa.2013.0819.

Iverson RM, Logan M, LaHusen RG, Berti M. 2010. The perfect debris flow? Aggregated results from 28 large-scale experiments. *Journal of Geophysical Research* **115**: F03005. https://doi.org/10.1029/2009jf001514.

Iverson RM, Schilling SP, Vallance JW. 1998. Objective delineation of lahar-inundation hazard zones. *Geological Society of America Bulletin* **110**: 972–984. https://doi.org/10.1130/0016-7606(1998)110<0972:Odolih>2.3.Co;2.

Jakob M, Hungr O. 2005. *Debris-flow Hazards and Related Phenomena*. Springer Verlag: Berlin.

Johnson AC, Swanston DN, McGee KE. 2000. Landslide initiation, runout, and deposition within clearcuts and old-growth forests of Alaska. *Journal of the American Water Resources Association* **36**: 17–30. https://doi.org/10.1111/j.1752-1688.2000.tb04245.x.

Johnson AC, Wilcock P. 2002. Association between cedar decline and hillslope stability in mountainous regions of southeast Alaska. *Geomorphology* **46**: 129–142. https://doi.org/10.1016/S0169-555X(02)00059-4.

Karl SM. 1999. Preliminary Geologic Map of Northeast Chichagof Island, Alaska. US Geological Survey Open-file Report, 96-53. US Geological Survey: Reston, VA. DOI: https://doi.org/10.3133/ofr9653.

Karl SM, Haeussler PJ, Himmelberg GR, Zumsteg CL, Layer PW, Friedman RM, Roeske SM, Snee LW. 2015. *Geologic Map of Baranof Island, Southeastern Alaska*, US Geological Survey Scientific Investigations Report, Map 3335. US Geological Survey: Reston, VA; 82. DOI: https://doi.org/10.3133/sim3335.

Kaufman DS, Manley WF. 2004. Pleistocene maximum and Late Wisconsinan glacier extents across Alaska, USA. In *Quaternary Glaciations – Extent and Chronology, Part II: North America*, Ehlers J, Gibbard PL (eds). Elsevier: Amsterdam; 9–27.

Kean JW, McCoy SW, Tucker GE, Staley DM, Coe JA. 2013. Runoff-generated debris flows: observations and modeling of surge initiation, magnitude, and frequency. *Journal of Geophysical Research: Earth Surface* **118**: 2190–2207. https://doi.org/10.1002/jgrf.20148.

Lancaster ST, Hayes SK, Grant GE. 2001. Modeling sediment and wood storage and dynamics in small mountainous watersheds. In *Geomorphic Processes and Riverine Habitat*, Dorava JM, Montgomery DR, Palcsak BB, Fitzpatrick FA (eds). American Geophysical Union: Washington, DC; 85–102.

Lancaster ST, Hayes SK, Grant GE. 2003. Effects of wood on debris flow runout in small mountain watersheds. *Water Resources Research* **39**: 1168. https://doi.org/10.1029/2001WR001227.

Legros F. 2002. The mobility of long-runout landslides. *Engineering Geology* **63**: 301–331. https://doi.org/10.1016/S0013-7952(01)00090-4.

Major JJ. 2000. Gravity-driven consolidation of granular slurries: implications for debris-flow deposition and deposit characteristics. *Journal of Sedimentary Research* **70**: 64–83. https://doi.org/10.1306/2DC408FF-0E47-11D7-8643000102C1865D.

Major JJ, Iverson RM. 1999. Debris-flow deposition: effects of pore-fluid pressure and friction concentrated at flow margins. *Geological Society of America Bulletin* **111**: 1424–1434. https://doi.org/10.1130/0016-7606(1999)111<1424:Dfdeop>2.3.Co;2.

Mann DH. 1986. Wisconsin and Holocene glaciation of southeast Alaska. In *Glaciation in Alaska: The Geologic Record*, Hamilton TD, Reed KM, Thorsen RM (eds). Alaska Geological Society: Anchorage, AK.

Mann DH, Hamilton TD. 1994. Late Pleistocene and Holocene paleoenvironments of the North Pacific coast. *Quaternary Science Reviews* **14**: 449–471. https://doi.org/10.1016/0277-3791(95)00016-I.

May CL, .2002. Debris flows through different forest age classes in the central Oregon Coast Range. *Journal of the American Water Resources Association* **38**: 1097–1113. https://doi.org/10.1111/j.1752-1688.2002.tb05549.x.

May CL, Gresswell RE. 2004. Spatial and temporal patterns of debris-flow deposition in the Oregon Coast Range, USA. *Geomorphology* **57**: 135–149. https://doi.org/10.1016/s0169-555x(03)00086-2.

Middleton G. 1970. Experimental Studies Related to the Problem of Flysch Sedimentation, Geological Association of Canada Special Papers, 7. The Geological Association of Canada: St John's; 253–272.

Montgomery DR, Massong TM, Hawley SC. 2003. Influence of debris flows and log jams on the location of pools and alluvial channel reaches, Oregon Coast Range. *Geological Society of America Bulletin* **115**:78–88. https://doi.org/10.1130/0016-7606(2003)115<0078:IODFAL>2.0.CO;2.

Pan Y, Chen JM, Birdsey R, McCullough K, He L, Deng F. 2011. Age structure and disturbance legacy of North American forests. *Biogeosciences* **8**: 715–732. https://doi.org/10.5194/bg-8-715-2011.

Penserini BD, Roering JJ, Streig A. 2017. A morphologic proxy for debris flow erosion with application to the earthquake deformation cycle, Cascadia Subduction Zone, USA. *Geomorphology* **282**: 150–161. https://doi.org/10.1016/j.geomorph.2017.01.018.

Pierson TC. 1985a. Effects of slurry composition on debris flow dynamics, Rudd Canyon, Utah. In *Delineation of Landslide, Flash Flood, and Debris Flow Hazards in Utah*, Bowles DS (ed). Utah State University Water Research Laboratory, General Series Report UWRL/G-85/0. Utah Water Research Laboratory: Logan, UT.

Pierson TC. 1985b. Initiation and flow behavior of the 1980 Pine Creek and Muddy river lahars, Mount St. Helens, Washington. *Geological Society of America Bulletin* **96**: 1056–1069. https://doi.org/10.1130/0016-7606(1985)96<1056:IAFBOT>2.0.CO;2.

Ping CL, Shoji S, Ito T, Takahashi T, Moore JP. 1989. Characteristics and classification of volcanic-ash-derived soils in Alaska. *Soil Science* **148**: 8–28. https://doi.org/10.1097/00010694-198907000-00002.

Pudasaini SP. 2012. A general two-phase debris flow model. *Journal of Geophysical Research: Earth Surface* **117**(F3): F03010. https://doi.org/10.1029/2011JF002186.

Radjai F, Wolf DE, Jean M, Moreau J-J. 1998. Bimodal character of stress transmission in granular packings. *Physical Review Letters* **80**: 61-64. https://doi.org/10.1103/PhysRevLett.80.61.

Rickenmann D. 1999. Empirical relationships for debris flows. *Natural Hazards* **19**: 47–77. https://doi.org/10.1023/A:1008064220727.

Rickenmann D. 2005. Runout prediction methods. In *Debris-flow Hazards and Related Phenomena*, Jakob M, Hungr O (eds). Springer Verlag: Berlin.

Rickenmann D, Zimmermann M. 1993. The 1987 debris flows in Switzerland: documentation and analysis. *Geomorphology* **8**(2–3): 175–189. https://doi.org/10.1016/0169-555X(93)90036-2.

Riehle JR. 1996. *The Mount Edgecumbe Volcanic Field, A Geologic History*, USDA Forest Service Alaska Region R10-RG-114 and US Geologic Survey. US Geological Survey: Reston, VA.

Riehle JR, Mann DH, Peteet DM, Engstrom DR, Brew DA, Meyer CE. 1992. The Mount Edgecumbe tephra deposits, a marker horizon in southeastern Alaska near the Pleistocene-Holocene boundary. *Quaternary Research* **37**: 183–202. https://doi.org/10.1016/0033-5894(92)90081-S.

Rosato A, Strandburg KJ, Prinz F, Swendsen RH. 1987. Why the Brazil nuts are on top: size segregation of particulate matter by shaking. *Physical Review Letters* **58**: 1038–1040. https://doi.org/10.1103/PhysRevLett.58.1038.

Ruefenacht B, Finco M, Nelson M, Czaplewski R, Helmer E, Blackard J, Holden G, Lister A, Salajanu D, Weyermann D. 2008. Conterminous US and Alaska forest type mapping using forest inventory and analysis data. *Photogrammetric Engineering and Remote Sensing* **74**: 1379–1388. https://doi.org/10.14358/PERS.74.11.1379.

Savage SB, Sayed M. 1984. Stresses developed by dry cohesionless granular materials sheared in an annular shear cell. *Journal of Fluid Mechanics* **142**: 391–430. https://doi.org/10.1017/S0022112084001166.

Scheidl C, Rickenmann D. 2010. Empirical prediction of debris-flow mobility and deposition on fans. *Earth Surface Processes and Landforms* **35**: 157–173. https://doi.org/10.1002/esp.1897.

Schroeder WL. 1983. *Geotechnical Properties of Southeast Alaskan Forest Soils*. Oregon State University Civil Engineering Department, USDA Forest Service: Corvallis, OR.

Shaw JD. 2000. Application of stand density index to irregularly structured stands. *Western Journal of Applied Forestry* **15**: 40–42.

Shulski M, Wendler G. 2007. *The Climate of Alaska*. University of Alaska Press: Fairbanks, AK.

Simoni A, Mammoliti M, Berti M. 2011. Uncertainty of debris flow mobility relationships and its influence on the prediction of inundated areas. *Geomorphology* **132**: 249–259. https://doi.org/10.1016/j.geomorph.2011.05.013.

Sitka GeoTask Force. 2016. *Summaries: August 2015 Sitka Landslides*, Vol. **32**. Sitka Sound Science Center: Sitka, AK; 1.

Stock JD, Dietrich WE. 2003. Valley incision by debris flows: evidence of a topographic signature. *Water Resources Research* **39**:1089. https://doi.org/10.1029/2001wr001057.

Stock JD, Dietrich WE. 2006. Erosion of steepland valleys by debris flows. *Geological Society of America Bulletin* **118**: 1125–1148. https://doi.org/10.1130/b25902.1.

Sun Q, Jin F, Liu J, Zhang G. 2010. Understanding force chains in dense granular materials. *International Journal of Modern Physics B* **24**: 5743–5759. https://doi.org/10.1142/s0217979210055780.

Suwa H, Okuda S. 1983. Deposition of debris flows on a fan surface Mt. Yakedake, Japan. *Zeitschrift fur Geomorphologie* **46**: 79–101.

Swanston DN. 1969. *Mass Wasting in Coastal Alaska, USDA Forest Service Research Paper PNW-83*. Juneau, AK: Institute of Northern Forestry.

Swanston DN. 1970. Mechanics of debris avalanching in shallow till soils of southeast Alaska. In *USDA Forest Service Research Paper PNW, 103*. US Forest Service: Washington, DC.

Swanston DN. 1974. Soil mass movement. In *In The Forest Ecosystem of Southeast Alaska, Harris AS, Farr WA (eds), USDA Forest Service General Technical Report PNW-25*. US Forest Service: Washington, DC.

Swanston DN, Marion DA. 1991. Landslide response to timber harvest in southeast Alaska. In *Proceedings of the Fifth Federal Interagency Sedimentation Conference*, Las Vegas, NV; 7.

US Department of Agriculture Forest Service. 2018. *Tongass Landslide Areas. ESRI Geodatabase*. US Forest Service: Washington, DC.

Vallance JW, Savage SB. 2000. Particle segregation in granular flows down chutes. In *IUTAM Symposium on Segregation in Granular flows*, Rosato A, Blackmore DL (eds). Springer: Cape May, NJ; 31–51.

VanDine D. 1996. *Debris Flow Control Structures for Forest Engineering*, Research Branch, Working Paper 08/1996. Victoria, BC: British Columbia Ministry of Forestry.

Webb RH, Magirl CS, Griffiths PG, Boyer DE. 2008. *Debris Flows and Floods in Southeastern Arizona from Extreme Precipitation in July 2006 – Magnitude, Frequency, and Sediment Delivery*, US Geological Survey Open-file Report, 2008-1274. *US Geological Survey: Reston, VA*;1–103. https://doi.org/10.3133/ofr20081274.

Yu F-C, Chen C-Y, Chen T-C, Hung F-Y, Lin S-C. 2006. A GIS process for delimitating areas potentially endangered by debris flow. *Natural Hazards* **37**: 169–189. https://doi.org/10.1007/s11069-005-4666-8.